the Fourier map, the presence of four OH···O bonds can be inferred from a consideration of interatomic distances. Each molecule is hydrogen-bonded to four neighbours.

O(1) ···O(2^{i})	2·99 (3) Å	[O(2^{i}): x, $1+y$, z]
O(1′)···O(2^{ii})	2·92 (2)	[O(2^{ii}): $-x$, $1+y$, $\frac{1}{2}-z$]
O(2) ···O(1^{iii})	2·99 (3)	[O(1^{iii}): x, $-1+y$, z]
O(2′)···O(1^{iv})	2·92 (2)	[O(1^{iv}): $-x$, $-1+y$, $\frac{1}{2}-z$]

The atoms denoted by a prime are related to the atoms listed in Table 2 by the twofold rotation axis.

This work was supported by the National Research Council of Canada in the regional development program. The author wishes to acknowledge Drs F. D. Rochon and Y. Pépin for taking interest in this work. Thanks are due to Dr P. Richard for useful discussion and Messrs Jean-François Guédon and Placide Massé for their cooperation at the University Computing Center.

References

AHMED, F. R. (1970). *Crystallographic Computing*, pp. 255–294. Copenhagen: Munksgaard.

COTTON, F. A. & WILKINSON, G. (1972). *Advanced Inorganic Chemistry*, 3rd ed., p. 730. London: Interscience.

DAUBEN, C. H. & TEMPLETON, D. H. (1959). *Acta Cryst.* **8**, 841–842.

DAVIES, B. W. & PAYNE, N. C. (1974). *Inorg. Chem.* **13**, 1848–1853.

International Tables for X-ray Crystallography (1968). Vol. III, 2nd ed., pp. 202–276. Birmingham: Kynoch Press.

International Tables for X-ray Crystallography (1969). Vol. I, 3rd ed., p. 101. Birmingham: Kynoch Press.

JOHNSON, C. K. (1970). *ORTEP*. Oak Ridge National Laboratory Report ORNL-3794.

MANOJLOVIĆ-MUIR, L., MUIR, K. W. & IBERS, J. A. (1969). *Discuss. Faraday Soc.* **47**, 84–92.

ROCHON, F. D. & THEOPHANIDES, T. (1972). *Canad. J. Chem.* **50**, 1325–1330.

STEWART, J. M., KRUGER, G., AMMON, H., DICKINSON, C. H. & HALL, S. R. (1972). X-RAY 72 Program System. Technical Report TR-192, Computer Centre, Univ. of Maryland, College Park, Maryland, U.S.A.

Acta Cryst. (1975). B**31**, 1864

Pentaerythritol Tetranitrate II: Its Crystal Structure and Transformation to PETN I; an Algorithm for Refinement of Crystal Structures with Poor Data*

BY HOWARD H. CADY AND ALLEN C. LARSON†

University of California, Los Alamos Scientific Laboratory, Los Alamos, New Mexico 87544, *U.S.A.*

(*Received* 21 *January* 1974; *accepted* 6 *January* 1975)

The crystal structure of the high-temperature polymorph of pentaerythritol tetranitrate ($C_5H_8N_4O_{12}$) has been determined from the intensity data on one rotation photograph. PETN II crystallizes in space group *Pcnb* ($a=13{\cdot}29$, $b=13{\cdot}49$, and $c=6{\cdot}83$ Å) with four molecules per unit cell and a calculated density of 1·72 g cm^{-3} at 136°C. The intensity data are insufficient for a normal structure determination so that bond distance and angle information from the structure of PETN I and repulsion terms were included as constraints in the least-squares refinement. The geometries of the PETN molecules in PETN I and II are nearly identical. A mechanism is proposed for the observed PETN II to PETN I transformation that accounts for the observed rates of transformation, low activation energy, and correlation between the structures of the polymorphs. The authors believe that this refinement algorithm has great potential for the refinement of crystal structures from powder data when the molecular structure is known.

Introduction

Two polymorphs of the important explosive pentaerythritol tetranitrate ($C_5H_8N_4O_{12}$) were first reported by Blomquist & Ryan (1944). The common form, PETN I, was thought to be stable to the melting point (142·9°C) even though no transformation of PETN II to PETN I was observed above 130°C. Careful measurement of the melting points of the two polymorphs shows that PETN II actually melts 0·2°C higher than PETN I and hence PETN II must be the stable polymorph at the melting point. The observation of Blomquist & Ryan (1944) that PETN II transforms rapidly to PETN I at temperatures below 130°C is easily confirmed.

The heat of fusion of PETN I is very dependent on the crystallization technique and varies from 38 cal g^{-1} for single, well-formed crystals to 32 cal g^{-1} for rapidly precipitated fine crystals. The melting point of the

* This work was performed under the auspices of the U. S. Atomic Energy Commission.

† Present address: 913 Dartmoor Dr., Austin, TX 78746, U.S.A.

rapidly precipitated PETN I is a function of the heating rate, and final liquidus temperatures as low as 137°C have been observed at high heating rates.

Small changes in the X-ray diffraction patterns accompany the changes in heat of fusion, and more pronounced changes occur when dipentaerythritol hexanitrate (diPEHN) or tripentaerythritol octanitrate (triPEON) is incorporated by solid solution in the crystals. An extensive study of the PETN–diPEHN–triPEON system has been made by Cady (1972). These changes could not be explained using the known structure of PETN I [Booth & Llewellyn (1947), further refined by Trotter (1963), with the original data].

Microscopic hot-stage studies of the PETN II to PETN I solid–solid polymorphic transformation showed that there is a definite relationship between the crystallographic axes of the two polymorphs. This transformation is inhibited by impurities trapped in the crystal. The high correlation between the structures of PETN I and II indicates that an X-ray diffraction study of PETN II might provide an insight into the variations in the thermal stability, heats of fusion, rates of annealing, and diffraction patterns of various PETN samples.

Initially it was hoped that a powder pattern of PETN II could be obtained and the line intensities would explain the observed intensity changes in various PETN I samples. The powder pattern obtained [Fig. 1(*c*)] was closely related to an aligned single crystal rotation pattern and comparison with Fig. 1(*b*) and (*d*) confirmed the correlation of the PETN II and PETN I unit cells. Eventually Fig. 1(*c*) was indexed and the probable space groups determined. The apparent space group, trial structure, and possible transformation mechanism were assigned simultaneously by considering the observed extinctions, the nature of the transformation as observed with an optical microscope, molecular packing requirements, the known PETN I structure, and chemical bonding, and by requiring any proposed model to be consistent with the observations. Calculated diffraction intensities from the first self-consistent model devised matched reasonably with the intensities of Fig. 1(*c*) and no further effort was made to find alternative models. Concurrently with the work on PETN II one of us (A.C.L.) was developing procedures for incorporating interatomic distance information in crystal-structure refinements by least-squares techniques. The refinement of this under-determined structure seemed to be an ideal test problem for the procedure.

Experimental

X-ray diffraction patterns can only be obtained from PETN II when the temperature of the sample is maintained above 130°C because of the rapid transformation to PETN I at lower temperatures. The temperature of the sample must also be substantially less than 142°C because of the rapid decomposition of PETN in the melt and resulting autocatalytic decomposition of the sample by nonvolatile decomposition products that depress the melting point. A single-crystal X-ray precession camera was modified to obtain powder patterns rapidly on flat-type 57-Polaroid film from samples whose temperatures could be controlled within ±2°C. A sample of PETN I was placed in a 0·3 mm diameter thin-walled glass capillary. After obtaining a room-temperature diffraction pattern, the sample was heated to 144°C and cooled rapidly to 136°C. An X-ray diffraction pattern of the PETN II that recrystallized from the melt was obtained, after which the sample was cooled at 6°C min^{-1} to room temperature and another diffraction pattern was taken. Diffraction patterns taken with Ni-filtered Cu $K\alpha$ radiation ($\lambda = 1{\cdot}5418$ Å) of (*a*) the PETN sample before heating, (*b*) a single crystal of PETN I, (*c*) PETN II at 136°C, and (*d*) PETN I obtained by cooling PETN II are shown in Fig. 1. The orientation effects of recrystallization in a capillary (**c** parallel to the capillary axis) and high correlation between PETN II and its PETN I transformation product are obvious. The halos at the outer edges of Fig. 1(*a*), (*c*), and (*d*) are caused by diffraction from a nickel foil that was part of the apparatus.

The pattern reproduced in Fig. 1(*c*) was indexed by trial and error. The pattern could almost be indexed with a tetragonal cell but the inconsistencies were too great to be ignored and eventually an orthorhombic cell consistent with all the observed lines was determined. Careful measurement of line positions was used to assist in determining extinctions as well as cell dimensions. Fig. 1 is included to emphasize the poor quality and paucity of the data; however, the originals are obviously better than these reproductions. Polaroid film is not a satisfactory medium for collecting intensity information and would not have been used if we had been able to repeat the original experiment. The final choice of space group *Pcnb* is reasonable since it only requires the insertion of a center of symmetry into *Pcn*2 which is in turn a subgroup of $P\bar{4}2_1c$. This is in effect the replacement of the 2_1 axis in the tetragonal space group by a glide plane.

The unit-cell parameters for PETN I, given in Table 1, compare favorably with those of Booth & Llewellyn (1947) and with the values $a = 9{\cdot}380$ and $c = 6{\cdot}709$ Å determined by conventional powder-pattern techniques using a 114·57 mm diameter X-ray powder camera.

Diffraction intensities for each of the three data sets [Fig. 1(*b*), (*c*), and (*d*)] were divided visually into ten classes. The numerical value for each class from Fig. 1(*d*) was determined by averaging the intensities calculated, from the known PETN I structure, for every reflection assigned to that class. The same numerical values were assigned to the corresponding intensity classes of Fig. 1(*b*) and (*c*). Intensities of unresolved reflection pairs from Fig. 1(*c*) were divided in proportion to the calculated intensities from the trial PETN II structure. Unscaled structure factors were calculated by correcting the intensities for Lorentz, polarization,

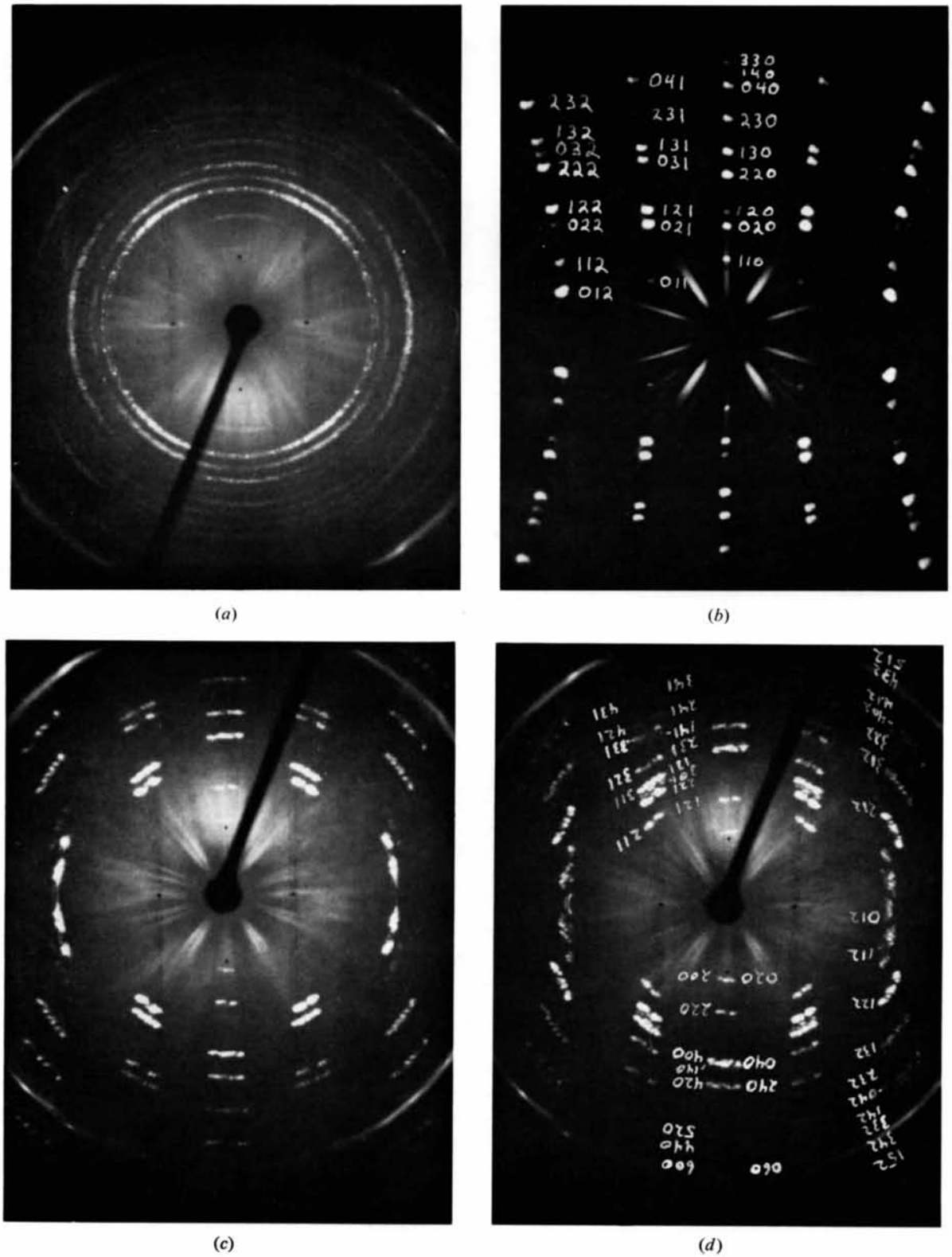

(a) (b)

(c) (d)

Fig. 1. X-ray diffraction patterns of PETN. (*a*) Powder before heating (PETN I). (*b*) Single crystal of PETN I rotated about the *c* axis. (*c*) PETN II crystals at 136°C (recrystallized from melt). (*d*) PETN I formed by cooling sample in (*c*) to room temperature.

[*To face p.* 1865

Table 1. *Crystal data for PETN from measurements of Fig. 1*

	PETN I (22 °C)	PETN II (136 °C)
Unit-cell parameters		
a	9·38 Å	13·29 Å
b	9·38	13·49
c	6·71	6·83
Z	2	4
D_x	1·778 g cm^{-3}	1·716 g cm^{-3}
D_m (flotation)	1·778 g cm^{-3}	
Systematic extinctions	$hkl, l=2n+1$	$0kl, l=2n+1$
	$h00, h=2n+1$	$h0l, h+l=2n+1$
		$hk0, k=2n+1$
Space group	$P\bar{4}2_1c$	$Pcnb$
Equivalent positions	x,y,z	x,y,z
	$\bar{x},\bar{y},z$	$\bar{x},\frac{1}{2}-y,z$
	$\frac{1}{2}-y,\frac{1}{2}-x,\frac{1}{2}+z$	$\frac{1}{2}-x,y,\frac{1}{2}+z$
	$\frac{1}{2}+y,\frac{1}{2}+x,\frac{1}{2}+z$	$\frac{1}{2}+x,\frac{1}{2}-y,\frac{1}{2}+z$
	$y,x,\bar{z}$	$x,\frac{1}{2}+y,\bar{z}$
	$\bar{y},\bar{x},\bar{z}$	$\bar{x},\bar{y},\bar{z}$
	$\frac{1}{2}-x,\frac{1}{2}+y,\frac{1}{2}-z$	$\frac{1}{2}-x,\frac{1}{2}+y,\frac{1}{2}-z$
	$\frac{1}{2}+x,\frac{1}{2}-y,\frac{1}{2}-z$	$\frac{1}{2}+x,\bar{y},\frac{1}{2}-z$

and multiplicity factors only. The reflections were arbitrarily assigned weights equal $1/(2+I)$ where I, the observed intensity, runs from 1 for the weakest observed reflection to 98 for the strongest reflection.

Structure solution and refinement

A model for the crystal structure of PETN II was obtained from the known structure of PETN I, the observations that the c unit-cell dimensions of PETN I and PETN II are nearly identical and that a and b unit-cell dimensions of PETN II are almost equal to the length of the [110] unit-cell diagonal of PETN I, and the assumption that no intermolecular contacts will be less than a normal van der Waals contact distance. The space-group symmetry changes between PETN I and PETN II require changing half of the molecules into their mirror images by bond rotations. The PETN II structure no longer requires $\bar{4}$ symmetry in the molecule; however, a molecule with $\bar{4}$ symmetry fits well, and this symmetry is nearly retained. Van der Waals repulsions require alternate layers of molecules (perpendicular to **b**) to translate about 1 Å in a direction parallel to **c**. The atom locations from this model structure were used as input positions in the least-squares refinement.

Only 42 unique observed reflections are available to determine the 43 positional, 15 isotropic thermal, and scale parameters of the structure. The structure would be indeterminate with a normal refinement, so the least-squares program was modified to include additional equations of condition based upon interatomic distances. The two types of interatomic distance constraints used were bond-length constraints of the type suggested by Waser (1963) and Rollett (1970), and a crude form for van der Waals repulsion. 'Bond length' constraints force the structure to have reasonable bond angles and distances, while atoms not involved in covalent bonds are forced apart by the repulsion terms. The function minimized was

$$\sum_{hkl} w_{hkl}(|F_o|_{hkl}-|F_c|_{hkl})^2 + a\sum_{ij\ \text{bond}} w_{ij}(d_{ij}-L_{ij})^2 + b\sum_{ij\ \text{repel}} (D_{ij}/d_{ij})^6.$$

The symbols in the sum over hkl have their conventional meanings. The formula for estimating $w_{hkl}[=1/(2+I_{hkl})]$ has already been described in the experimental section. The thermal parameters were considered relatively unimportant; they were therefore assigned reasonable but arbitrary values and were held fixed during the refinement. Atomic scattering factors published by Doyle & Turner (1968) were used for nonhydrogen atoms, and the spherical H-atom approximation of Stewart, Davidson & Simpson (1965) was used for hydrogen atoms.

In the sum over ij bond, the 46 observed interatomic distances, L_{ij}, that determine bond lengths and angles (angles are determined by next-nearest atom distances) in the structure were assumed to have the lengths found by Trotter (1963) in PETN I except that the central carbon was assumed to be tetrahedrally bonded and the hydrogen atoms were placed in appropriate positions 1·05 Å from the other carbon atoms. The $w_{ij}(=1/\sigma^2_{L_{ij}})$ terms were calculated from assumed standard deviations of these interatomic distances. These standard deviations were assumed to be 0·04 Å except for C–C, C–H, and H–H distances, which were 0·03, 0·05, and 0·06 Å, respectively. The term d_{ij} is the distance from atom i to atom j calculated from the refinement parameters.

The sum over ij repel attempts to minimize the overlap of nonbonded atoms. D_{ij} is the assumed contact distance and is based on radii of 1·57, 1·50, 1·40, and 1·20 Å for carbon, nitrogen, oxygen, and hydrogen atoms, respectively. The computed distance from atom i to atom j is again d_{ij}. Nonbonded atom repulsions were considered significant if the atoms were within 1·5 D_{ij} of each other, and the sum adds an additional 185 'observational equations', 67 of which were intramolecular repulsions. The choice of this function was based on the computational ease and has no real physical significance. Other reasonable functions could have been used.

The value of the parameter a in the function minimized is normally chosen so as to 'correct' absolute weights on distance equations to the scale of the relative weights in the hkl data. Here, however, our goodness of fit is imaginary and we set a equal to 6·0. A value of 6·0 was also chosen for b. These choices were made in an effort to make the average of the terms in each sum approximately equal. This is done so that the structure is determined more or less equally by each of the 'observations'. The refinement converged to a conventional R value ($\sum||F_o|-|F_c||/|F_o|$) of 0·14 for the hkl intensity data. This value indicates a valid structure when one considers the low quality of the data and the restrictions placed on the refinement. An independent check of the

least-squares refinement was obtained from calculated, observed, and difference Fourier maps. These maps are not well resolved, but do not indicate any systematic error in the structure. The observed Fourier map is shown in Fig. 2.

Final values of the least-squares parameters and their estimated standard deviations are given in Table 2. The observed and calculated structure factors are listed in Table 3.

Table 2. *Final least-squares parameters and their estimated standard deviations for PETN* II

The standard deviations apply to the last digits of the least-squares parameter. Fixed parameters have no stated standard deviation. The positional parameters are $\times 10^4$.

	x	y	z	B (Å^2)
C(1)	0	25	1738 (64)	2·5
C(2)	921 (9)	2295 (22)	3042 (64)	3·4
C(3)	−207 (22)	1590 (8)	444 (65)	3·4
N(1)	1455 (29)	1052 (57)	5366 (117)	3·4
N(2)	−1442 (69)	1089 (30)	−1957 (112)	3·4
O(1)	677 (28)	1471 (40)	4280 (94)	3·6
O(2)	−1002 (44)	1846 (28)	−883 (90)	3·6
O(3)	1149 (36)	474 (37)	6588 (73)	5·3
O(4)	−1965 (39)	1404 (34)	−3273 (73)	5·3
O(5)	2330 (28)	1212 (40)	4880 (79)	5·1
O(6)	−1244 (54)	224 (29)	−1592 (96)	5·1
H(1)	1533 (18)	2108 (56)	2185 (78)	6·0
H(2)	−447 (62)	1001 (20)	1301 (78)	6·0
H(3)	1077 (42)	2897 (33)	3914 (102)	6·0
H(4)	419 (32)	1406 (44)	−365 (112)	6·0

Table 3. *Observed and calculated structure factors for PETN* II

The column headings are k, $|F_o|$, and $|F_c|$. If $|F_o|$ is negative, the reflection is unobserved but estimated at ½ of the observation limit.

$h=0$ $l=0$			$h=1$ $l=2$			$h=2$ $l=0$			$h=3$ $l=1$			$h=4$ $l=2$		
0	0	648	1	36	37	0	47	28	0	71	77	0	76	62
2	61	30	2	−4	22	2	65	64	1	84	90	1	57	59
4	134	129	3	−20	31	4	82	65	2	−10	11	2	−6	21
6	33	38	4	113	98	6	−14	25	3	61	71	3	−21	28
			5	−27	19				4	42	50			
									5	−10	8			
$h=1$ $l=0$			$h=2$ $l=1$			$h=3$ $l=2$						$h=5$ $l=1$		
2	−12	13	1	65	68	1	69	67				0	−27	7
4	37	44	2	152	144	2	25	29				1	−4	5
6	−22	14	3	100	69	3	27	20				2	−14	2
			4	−13	3	4	21	20				3	−19	20
$h=1$ $l=1$			5	28	23									
0	−11	2	$h=2$ $l=2$			$h=4$ $l=0$						$h=5$ $l=2$		
1	−10	14	0	−15	9	0	130	135				1	90	72
2	39	26	1	23	27	2	79	63						
3	80	94	2	−14	11	4	65	47				$h=6$ $l=0$		
4	26	33	3	−7	7							0	33	36
5	−19	6	4	−17	20	$h=4$ $l=1$						2	−17	25
6	33	31				1	27	27						
						2	55	46				$h=6$ $l=1$		
						3	−9	2				1	−10	2
						4	66	53						

Table 4. *Bond lengths* (Å) *and angles* (°) *in PETN*

	PETN I (Trotter, 1963) Input to least-squares calculations	PETN II	PETN I single crystal	PETN I from PETN II
C(1)–C(2)	1·537	1·539	1·536	1·537
C(1)–C(3)		1·537		
C(2)–O(1)	1·462	1·433	1·434	1·427
C(3)–O(2)		1·433		
O(1)–N(1)	1·404	1·392	1·397	1·398
O(2)–N(2)		1·386		
N(1)–O(3)	1·203	1·212	1·207	1·206
N(2)–O(4)		1·203		
N(1)–O(5)	1·225	1·229	1·222	1·227
N(2)–O(6)		1·222		
C(2)–H(1)	1·05	1·03	1·03	1·03
C(3)–H(2)		1·04		
C(2)–H(3)		1·03	1·03	1·03
C(2)–H(4)		1·03		
C(2)–C(1)–C(2)	109·47	109·3	109·9	109·7
C(2)–C(1)–C(3)	109·47	109·4	109·2	109·3
C(2)–C(1)–C(3)	109·47	109·5	109·2	109·3
C(3)–C(1)–C(3)	109·47	109·8	109·9	109·7
C(1)–C(2)–O(1)	105·6	107·5	107·5	107·8
C(1)–C(2)–H(1)	109·0	110·0	110·0	110·1
C(1)–C(2)–H(3)	109·0	110·8	110·5	110·1
O(1)–C(2)–H(1)	105·0	108·9	108·5	109·1
O(1)–C(2)–H(3)	105·0	108·9	108·7	108·5
H(1)–C(2)–H(3)	109·0	111·2	111·6	111·1
C(1)–C(3)–O(2)	105·6	107·7	107·5	107·8
C(1)–C(3)–H(2)	109·0	110·0	110·0	110·1
C(1)–C(3)–H(4)	109·0	110·8	110·5	110·1
O(2)–C(2)–H(2)	105·0	108·4	108·5	109·1
O(2)–C(2)–H(4)	105·0	108·4	108·7	108·5
H(2)–C(2)–H(4)	109·0	111·5	111·6	111·1
C(2)–O(1)–N(1)	112·5	117·4	115·9	116·8
C(3)–O(2)–N(2)	112·5	117·9	115·9	116·8
O(1)–N(1)–O(3)	112·5	112·3	113·3	112·4
O(1)–N(1)–O(5)	117·1	119·2	117·8	118·5
O(3)–N(1)–O(5)	130·4	128·1	128·8	128·9
O(2)–N(2)–O(4)	112·5	112·1	113·3	112·4
O(2)–N(2)–O(6)	117·1	120·3	117·8	118·5
O(4)–N(2)–O(6)	130·4	127·5	128·8	128·9

The PETN I structure was also refined with the limited intensity data sets from Fig. 1(*b*) and (*d*) using equivalent constraints as a check of the method. Both data sets refined to R values less than 0·09 and indicate that the original PETN I data of Booth & Llewellyn (1947) may be of rather poor quality. The bond distances and angles found for PETN II and the two PETN I refinements are compared with the results of Trotter's (1963) refinement of Booth & Llewellyn's data ($R=0·153$) in Table 4. Surprisingly, the three structures agree with each other more than they agree with the previously published structure as far as bond lengths and angles are concerned. This may point to surprisingly good agreement between our sets of imprecise data, to errors in the Trotter structure, or to an unexpected efficiency of the repulsion terms in normalizing the molecular structure.

Only 20 of the 185 nonbonding repulsions indicate molecular contacts of less than the van der Waals contact distance, and all but three of these are intramolecular. The worst cases involve C(2)–O(5) and

C(3)–O(6) within-chain contacts, but even these are longer contacts than occur in Trotter's (1963) PETN I structure.

Fig. 3(*a*) is a stereo pair illustrating the molecular packing in PETN II, and Fig. 3(*b*) illustrates the packing in PETN I. The layer of molecules illustrated on the left-hand side of Fig. 3(*a*) and (*b*) is essentially identical for both structures, while the right-hand layers contain the differences in packing between PETN I and II. The major differences between the right-hand layers are that the CH_2ONO_2 groups rotate by somewhat less than 180° about the C–C bond, the entire molecule rotates nearly 60° about the *c* axis, and the molecular centers translate about 1 Å in the **c** direction.

The mechanism of the solid-state polymorphic transformation of PETN II to I can be elucidated by showing how these rotations and translations could occur. Assume a PETN II crystal oriented as in Fig. 3(*b*) with the *c* axis up and the *b* axis lying in the plane with positive direction to the right. Further assume a micro-

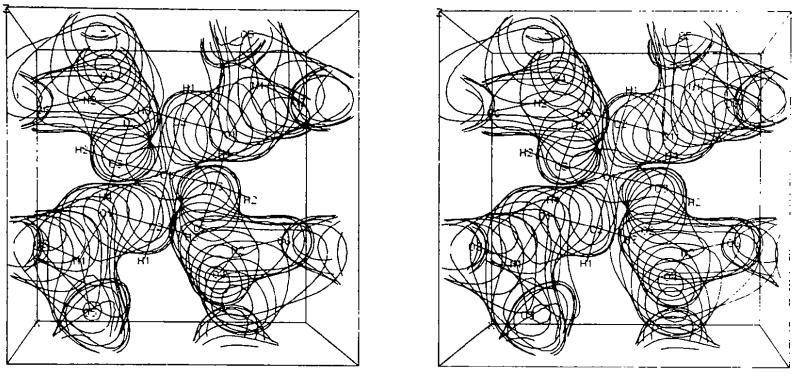

Fig. 2. Observed Fourier synthesis of PETN II at the 1·45 e Å^{-3} contour level. View is down the *c* axis and encloses the volume $-0{\cdot}25 \le x \le 0{\cdot}3$, $0{\cdot}0 \le y \le 0{\cdot}538$, and $-0{\cdot}435 \le z \le 0{\cdot}783$.

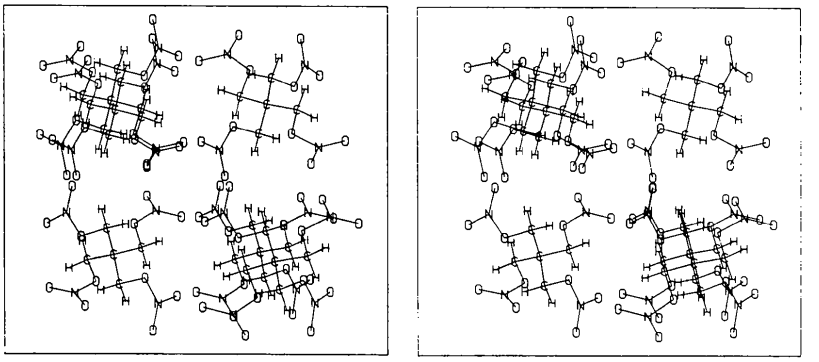

(*a*)

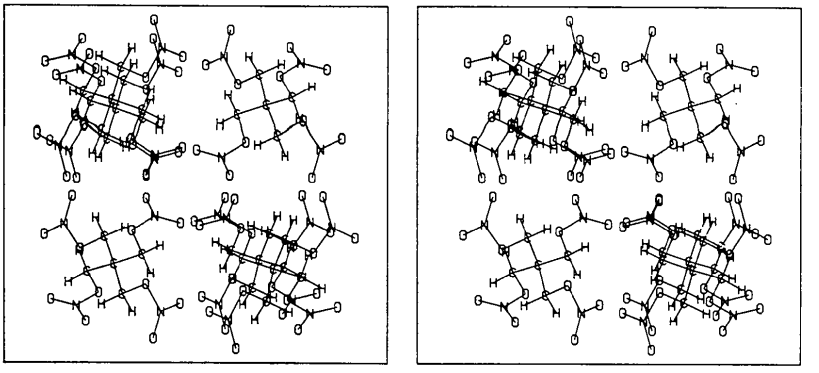

(*b*)

Fig. 3. (*a*) Molecular packing in PETN II as viewed down the *c* axis. (*b*) Molecular packing in PETN I as viewed down the *c* axis. The *a* axis runs diagonally.

scope with atomic resolution focused on a region like Fig. 3(*b*) with the PETN II to PETN I transformation zone moving upward into the region of focus. The layer of molecules to the left of the field of view remains unchanged as the transformation front climbs. As the transformation front moves into focus a 'tunnel' of activity would be observed, on the right, that when projected on the *a*,*b* plane has infinite length parallel to **a**, a width of about 6·7 Å parallel to **b**, and a maximum thickness of about 1 Å parallel to **c**. This tunnel is the result of the 1 Å translational difference between the molecular centers in PETN I and II. The nitrate groups of a PETN II molecule adjacent to the tunnel move into it, where they have room to rotate into the PETN I configuration. As this rotation is completed, the tunnel collapses as the transforming molecule moves toward the PETN I region. A new tunnel is then generated at the opposite end of the molecule, and the nitrate groups there have room to rotate, thus transferring a molecule from PETN II to PETN I while the tunnel moves with the transformation in the **c** direction. This type of transformation would propagate very rapidly in the *a*,*c* plane, as is observed.

The described transformation would transfer only one molecular layer in a perfect crystal. Crystal defects such as a screw axis parallel to **b** would provide an obvious mechanism for propagation in the **b** direction. Similarly crystal surfaces also provide a region where the transformation can propagate parallel to **b**. The observed rate of transformation parallel to **b** is much slower than in the *ac* plane as would be expected. The PETN II to I transformation has a low activation energy because none of the transformation steps involve strong intermolecular forces or require cooperative motions of several molecules simultaneously.

References

BLOMQUIST, A. T. & RYAN, J. F. JR (1944). *Studies Related to the Stability of PETN*. OSRD report NDRC-B-3566.

BOOTH, A. D. & LLEWELLYN, F. J. (1947). *J. Chem. Soc.* pp. 837–846.

CADY, H. H. (1972). *The PETN-DiPEHN-TriPEON System*, Los Alamos Scientific Laboratory report LA-4486-MS.

DOYLE, P. A. & TURNER, P. S. (1968). *Acta Cryst.* A**24**, 390–397.

ROLLETT, J. S. (1970). In *Crystallographic Computing*, edited by F. R. AHMED, pp. 170–171. Copenhagen: Munksgaard.

STEWART, R. F., DAVIDSON, E. R. & SIMPSON, W. T. (1965). *J. Chem. Phys.* **42**, 3175–3187.

TROTTER, J. (1963). *Acta Cryst.* **16**, 698–699.

WASER, J. (1963). *Acta Cryst.* **16**, 1091–1094.

Acta Cryst. (1975). B**31**, 1869

Structure Cristalline d'un Composé Nématogène: le (Méthoxybenzylidèneamino-4')-4 α-Méthyl Cinnamate de Propyle

PAR M. COTRAIT

Laboratoire de Cristallographie et de Physique cristalline, associé au CNRS, Université de Bordeaux I, 351 *cours de la Libération*, 33405 *Talence, France*

ET D. SY ET M. PTAK

Centre de Biophysique Moléculaire, CNRS, 45045 *Orléans Cedex, France*

(*Reçu le* 27 *janvier* 1975, *accepté le* 14 *février* 1975)

The crystal structure of a nematogenic compound, propyl 4-(4'-methoxybenzylideneamino)-α-methylcinnamate has been solved: it crystallizes in space group *Pbca* with $a=31{\cdot}358$, $b=15{\cdot}697$, $c=7{\cdot}749$ Å ($Z=8$). The chain is quite linear while the angle between the two phenyl rings is 36°. Molecules in the crystal are associated in pairs of enantiomers through $\bar{1}$ centres of symmetry, the binding energy for an isolated pair being as high as 7·8 kcal mol^{-1}.

Introduction

L'existence et les propriétés spécifiques des phases mésomorphes sont directement reliées à la nature des molécules qui les constituent. La composition chimique de ces molécules détermine leur conformation, leurs interactions, leur mobilité et leurs corrélations orientationnelles. La description des mésophases à l'échelle microscopique est complexe et n'a que peu progressé jusqu'à présent. Un premier pas dans ce domaine consiste à déterminer les conformations moléculaires et les interactions statiques dans le cristal, pour comprendre leurs modifications lors de transitions cristal → mésophase. Après les travaux préliminaires de Bernal & Crowfoot (1933), quelques structures cristallines de composés nématogènes ont été déterminées, notamment celles de l'anisaldéhyde-azine par Galigné & Falgueirettes (1968), du 4,4'-azodiphénétole par Ga-